Crystallographic Alignment of ZnO Nanorod Arrays on Zn_2GeO_4 Nanocrystals: Promising Lattice-Matched Substrates

Chaoyi Yan and Pooi See Lee*

School of Materials Science and Engineering, Nanyang Technological University, Singapore 639798, Singapore

Received: September 20, 2009; Revised Manuscript Received: November 01, 2009

We demonstrated that ternary Zn_2GeO_4 crystals could be used as potential lattice-matched substrates for ZnO nanorod array growth. Single-crystalline Zn_2GeO_4 nanowires were used as substrates for crystallographic alignment of ZnO nanorod arrays. Structural characterization verified the heteroepitaxial growth between the ZnO *c*-plane and Zn_2GeO_4 side facets, which was attributed to the small lattice mismatches. The semiconducting Zn_2GeO_4 crystals are of potential interest as novel alternative substrates for ZnO nanorod array growth.

1. Introduction

One-dimensional (1D) nanomaterials have been widely used as building blocks for nanoscale electronic and optoelectronic devices.[1,2] Especially, 1D ZnO nanostructures have found spectacular applications in various fields, such as ultraviolet (UV) lasers,[3] field-effect transistors (FETs),[4] light-emitting diodes (LEDs),[5] solar cells,[6] piezo-nanogenerators,[7] etc. From an application viewpoint, syntheses of aligned nanowire arrays are of great importance for the fabrication of nano-heterojunction device arrays. Vertically aligned ZnO nanowire arrays can be obtained by homoepitaxial growth on ZnO buffer layer[8] or Zn foils.[9] Heteroepitaxial growth was also demonstrated on Al_2O_3,[3] GaN and AlN,[10] and γ-$LiAlO_2$ and MgO[11] substrates with selected orientations. Closely matched symmetry and lattice constant between the substrates and nanowires are essential for epitaxial growth.[3,11]

In this report, we show that the novel ternary Zn_2GeO_4 crystals can be used as lattice-matched substrates for ZnO nanorod array growth. Due to the difficulty in obtaining Zn_2GeO_4 bulk substrates or thin films with uniform crystal structure,[12,13] the single-crystalline Zn_2GeO_4 nanowires can be used as ideal substrates for nanorod array growth and crystallographic investigations.[14] While the insulating substrates (such as Al_2O_3 and MgO) would inhibit their applications, nanoheterojunction devices based on ZnO nanowire array grown on semiconducting GaN substrate have been demonstrated recently.[15,16] Zn_2GeO_4 is a wide-band-gap semiconductor (E_g = 4.68 eV) with tunable optical properties.[12,13] It is believed that Zn_2GeO_4 crystals not only serve as substrates for epitaxial ZnO nanowire array growth but also can be integrated into future nanoscale electronic and optoelectronic heterojunction devices.

2. Experimental Section

The Zn_2GeO_4 nanowires were synthesized using a horizontal double-tube furnace (Figure S1, Supporting Information), as reported previously.[14] In brief, mixed ZnO, GeO_2, and carbon powder (~1 g, molar ratio of 2:1:3) were used as source materials for nanowire growth with the assistance of Au. The furnace was heated at 1000 °C for 60 min in Ar gas (1.9 mbar). The optimum growth temperature region for the Zn_2GeO_4 nanowires is 500−400 °C.

* Corresponding author. Phone: (65)-67906661. Fax: (65)-67909081. E-mail: pslee@ntu.edu.sg. E-mail: pslee@ntu.edu.sg.

A secondary growth process was carried out for ZnO branch growth on primary Zn_2GeO_4 nanowires. The as-grown Zn_2GeO_4 nanowires were used as substrates for branch growth without further treatment. Mixed ZnO and carbon powder (~0.5 g, molar ratio of 1:1) was used as source materials. Typically, the furnace temperature was increased to 1000 °C at a rate of 15 °C min^{-1} and kept there for 60 min. But Ar gas mixed with 10% O_2 (total pressure 2.2 mbar) was used as carrier gas for ZnO branch growth. The temperature for ZnO branch growth was ~520 °C.

Morphologies and structures of the products were characterized using field emission scanning electron microscopy (FE-SEM) and X-ray diffraction (XRD) with Cu Kα radiation (λ = 1.5418 Å). Detailed structure analyses were performed by transmission electron microscopy (TEM) equipped with energy dispersive spectroscopy (EDS). EDS line scanning analyses were performed using the scanning transmission electron microscopy (STEM) attachment. For all TEM and EDS analyses, the products were dispersed in ethanol by sonication for 30 s, and then the solution was dropped on a copper grid coated with holey carbon film. The samples were dried naturally in air before analyses.

3. Results and Discussion

Morphology of the primary Zn_2GeO_4 nanowires synthesized via the Au-catalyzed vapor−liquid−solid (VLS) method is shown in Figure 1a. Large quantities of nanowires can be observed on the Si substrate surface. The diameters of the nanowires are in the range of 20−100 nm, with lengths up to tens of micrometers. TEM image (Figure 1a, inset) shows the smooth nanowire surface and the catalyst particle at the growth front, verifying the VLS growth mechanism.[14] Thin ZnO nanorod branches were successfully grown on the primary Zn_2GeO_4 nanowires after a secondary vapor phase deposition process (Figure 1b−d). The primary Zn_2GeO_4 nanowires were uniformly covered with thin ZnO branches. Enlarged FE-SEM images of the heterostructures were shown in Figure 1c,d. Well-aligned ZnO branches showed preferential growth directions, which were all perpendicular to the Zn_2GeO_4 backbone nanowires. Six-fold symmetry of the branches can be clearly identified from the top (Figure 1c) and side (Figure 1d) views. The arrows and numbers in Figure 1c,d indicate three of the six directions of symmetry. The thin ZnO branches have uniform diameters ~20 nm. Lengths of the branches are in the range of 0.8−1.2 μm after 60 min growth.

10.1021/jp909068v
Published on Web 11/16/2009

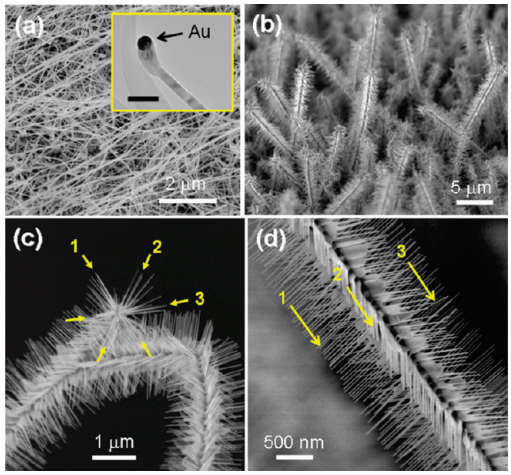

Figure 1. (a) FE-SEM image of the primary Zn_2GeO_4 nanowires. (b−d) FE-SEM images of the Zn_2GeO_4−ZnO nanowire heterostructures at different magnifications. The inset in part a is the TEM image showing the smooth nanowire surface and Au catalyst particle (dark region) at the growth front. The scale bar is 100 nm. The ZnO branches show 6-fold symmetry, as indicated in parts c and d.

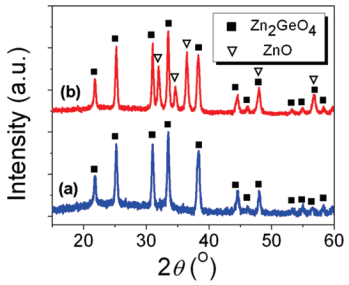

Figure 2. XRD patterns (a) before and (b) after the secondary branch growth. An additional ZnO phase was detected after the branch growth.

Crystal structures of the primary nanowires (before secondary growth) and heterostructures (after secondary growth) were characterized using XRD (Figure 2). The primary nanowires showed a pure Zn_2GeO_4 phase (Figure 2a) with rhombohedral crystal structure (JCPDS card 11-0687: $a = 14.231$ Å, $c = 9.53$ Å). No other impurity peaks were detected. After secondary growth, an additional ZnO phase with hexagonal crystal structure (JCPDS card 36-1451: $a = 3.2498$ Å, $c = 5.2066$ Å) was detected. The XRD results confirmed the addtional ZnO deposition on the Zn_2GeO_4 nanowire substrates. Together with the FE-SEM observations (Figure 1), it is evident that the heterostructures are composed of Zn_2GeO_4 backbones with ZnO branches.

TEM and EDS analyses were performed to characterize the structure and composition of the branched heterostructures in more detail. A typical TEM image of the branched heterostructure is shown in Figure 3a. Due to the specific 3D orientations of the heterostructure,[17] some ZnO branches appear oblique with respect to the Zn_2GeO_4 backbone (Figure 3a; see also Figure 1). A high-resolution TEM (HRTEM) image of the single-crystalline ZnO branch is shown in Figure 3b. The growth direction of the ZnO nanorod was along the *c*-axis of the hexagonal lattice, a typical growth direction for ZnO nanostructures.[3] EDS spectrum taken from the whole heterostructures (including backbone and branches) is shown in Figure 3c, revealing the presence of Zn, Ge, and O. Quantitative analysis showed that the atomic ratio of Zn/Ge was around 3.5/1. The higher Zn concentration than the stoichiometric value of pure

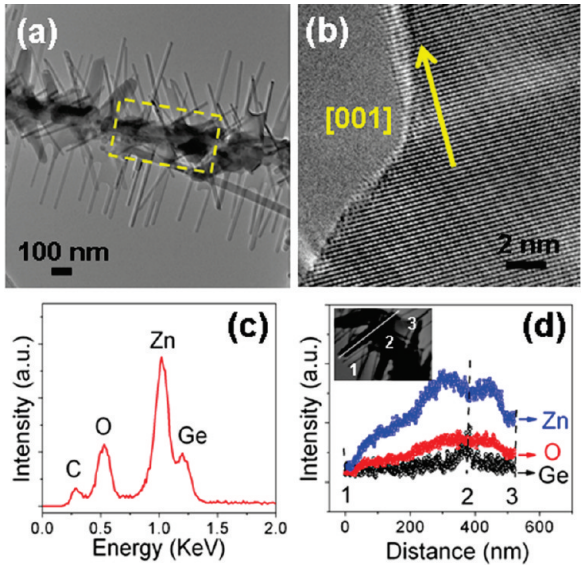

Figure 3. (a) Low-magnification TEM image of the branched heterostructures. The dashed rectangle highlights the ZnO shell surrounding the Zn_2GeO_4 nanowire. (b) HRTEM image of the ZnO branch. (c) EDS spectrum recorded from the whole heterostructure in part a. (d) EDS line scanning profiles revealing the Zn_2GeO_4 backbone nanowire with ZnO branches.

Zn_2GeO_4 (2/1) can be attributed to the presence of ZnO branches. EDS line scanning was performed to further verify the elemental distributions (Figure 3d). The scanning path is indicated by a white line in the STEM image (Figure 3d, inset), with number 2 denoting the position of the backbone Zn_2GeO_4 nanowire. The branch (from 1 to 2) is composed of Zn and O, and Ge can only be detected in the backbone nanowire (position 2). The elemental distribution in the line scanning profiles is consistent with XRD results, which showed ZnO growth on the Zn_2GeO_4 primary nanowires (Figure 2). It should be noted that a ZnO shell was found surrounding the primary Zn_2GeO_4 nanowire (as highlighted by the rectangle in Figure 3a), which was also observed in previous reports.[18,19] The EDS line scanning result with increasing Zn and O concentration around the Zn_2GeO_4 core also verifies the existence of the ZnO shell.

Previously, it was shown to be difficult to analyze the crystallographic relationship between the backbone nanowire and branches, due to the relatively thick ZnO shell deposition.[18] Here we chose Zn_2GeO_4 nanowires with very short ZnO branches (less than 20 nm, Figure 4a) to elucidate the heteroepitaxy. Note that the ZnO buffer layer was found to promote the growth of aligned nanowire arrays via homoepitaxial growth.[8,18] The Zn_2GeO_4 nanowires free of ZnO shell (Figure 4a−c) are essential to exclude the possibility of homoepitaxial growth. It can be clearly viewed that the short ZnO nanorods are perpendicular to the Zn_2GeO_4 backbone at the very early growth stage (see also Figure S3, Supporting Information). HRTEM images of the Zn_2GeO_4−ZnO interface revealing the detailed crystal structures are shown in Figure 4b−d (see also Figure 5). It is evident that the Zn_2GeO_4−ZnO interface is free of, for example, an amorphous sheath layer. The extension of clear lattice fringes from the Zn_2GeO_4 backbone to the ZnO branch reveals a crystalline interface, i.e., epitaxial growth. The Au-catalyzed Zn_2GeO_4 nanowires were found to grow along the [110] direction, with *c*-oriented ZnO nanorods grown on the $(1\bar{1}0)$ side facets (Figure 4d). The crystallographic relationship between the Zn_2GeO_4 backbone and ZnO branch are schematically presented in Figure 4g. An epitaxial growth

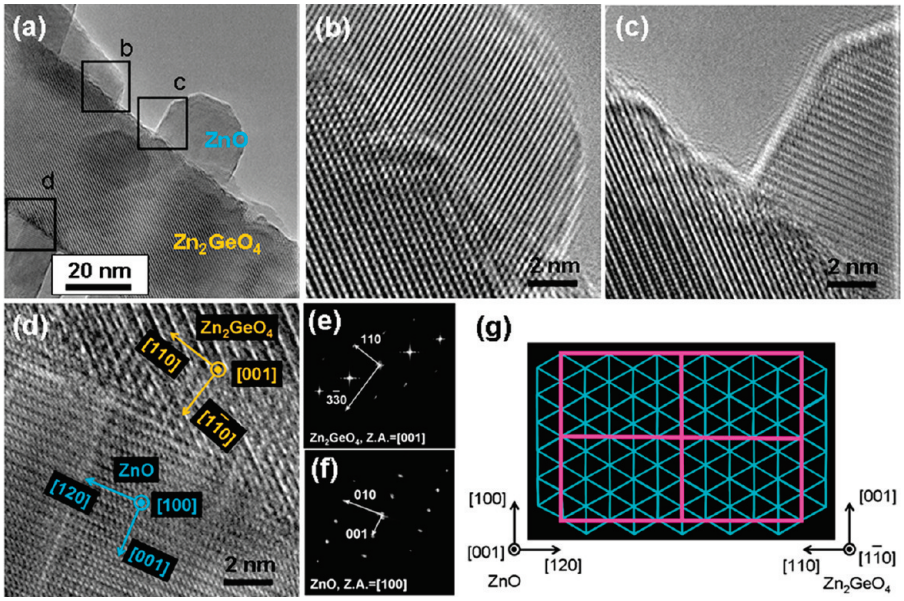

Figure 4. (a) TEM image of a Zn_2GeO_4 backbone with ZnO nuclei. (b−d) HRTEM images of the Zn_2GeO_4−ZnO interface, showing the epitaxial growth. (e, f) FFT patterns of the Zn_2GeO_4 backbone and ZnO branch, obtained from the HRTEM image in part d. (g) Schematic model of the epitaxial relationship between the (001) surface of ZnO and the (1$\bar{1}$0) surface of Zn_2GeO_4. The red rectangles show the lattices of the Zn_2GeO_4(1$\bar{1}$0) plane.

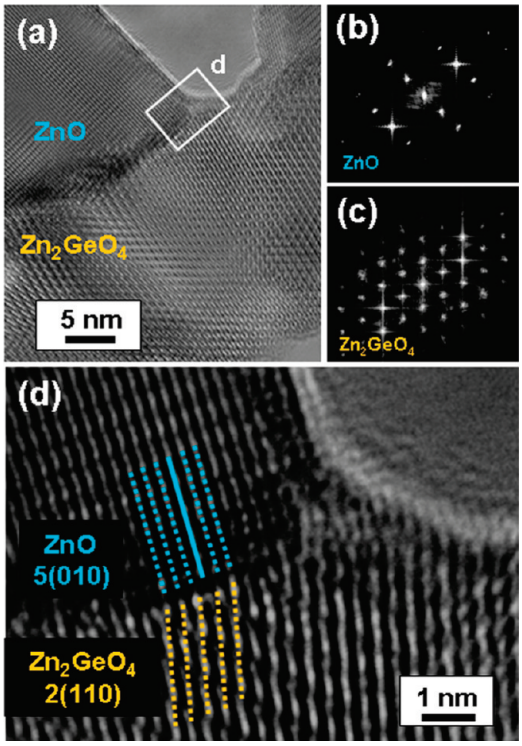

Figure 5. (a) HRTEM image of short ZnO branch grown on Zn_2GeO_4 nanowire. (b, c) FFTs of ZnO branch and Zn_2GeO_4 nanowire obtained from the HRTEM image in part a. (d) Enlarged view of the Zn_2GeO_4−ZnO interface showing the epitaxial relationship and misfit dislocations.

between the ZnO(001) plane and Zn_2GeO_4(1$\bar{1}$0) plane exists. Analogous to the Al_2O_3(110) plane,[3,20] the Zn_2GeO_4(1$\bar{1}$0) plane is a rectangular lattice with small lattice mismatches with the ZnO *c*-plane. The lattice mismatch between three [100] of ZnO (3 × 3.2498 = 9.749 Å) and [001] of Zn_2GeO_4 (9.53 Å) is 2.3%, and the mismatch along the ZnO[120] direction is only 1.1%. The small lattice mismatch is considered to be the main driving force of epitaxial growth in the process of minimizing the interfacial strain energy.

Structure defects such as misfit dislocations were observed at some of the Zn_2GeO_4−ZnO interfaces to relax strain and reduce the interfacial elastic energy. The dislocation formation was widely reported for crystal growth in lattice-mismatched systems.[21,22] As a typical example, a HRTEM image of the Zn_2GeO_4−ZnO interface with structure defects is show in Figure 5a. Growth directions of the ZnO and Zn_2GeO_4 are the same as those shown in Figure 4. An enlarged view of the interfacial region (marked by the square in Figure 5a) with misfit dislocations is shown in Figure 5d (indicated by dashed lines). The spacing for five (010) of ZnO (5 × 0.28 = 1.40 nm) is almost the same as two (110) of Zn_2GeO_4 (2 × 0.71 = 1.42 nm), as indicated in Figure 5d [note that the distance between dashed yellow lines is half of the spacing between Zn_2GeO_4 (110) planes]. Additional schematic diagrams of the crystallographic relationship are shown in Figure S2, Supporting Information.

The detailed growth processes of aligned ZnO nanorods on Zn_2GeO_4 backbones can be described as follows: During the secondary vapor deposition process, Zn vapor was generated at the central high-temperature region through carbothermal reactions. Instead of the direct gas conveyed in a conventional process, the Zn vapor would diffuse to the lower temperature region in a more stable manner due to the usage of the double-tube system (Figure S1, Supporting Information). Zn_2GeO_4 nanowires on top of Si substrates were located at the low-temperature region (400−500 °C) for ZnO deposition. The primary Zn_2GeO_4 nanowire surface is atomically rough and, thus, is an energetically favorable nucleation sites for ZnO.[18] At the initial growth stage, sparsely distributed ZnO nuclei are first deposited on the nanowire surface. The ZnO nuclei would preferentially elongate along the [001] direction due to the strong tendency of *c*-axial growth.[9,18,19] Driven by the epitaxial growth between ZnO *c*-plane and Zn_2GeO_4 side facets, the ZnO branches would grow perpendicularly to the Zn_2GeO_4 backbones. Meanwhile, apart from the longitude growth of ZnO branches, continuous ZnO deposition also resulted in the formation of thin ZnO shells surrounding the Zn_2GeO_4 core, as evidenced in Figure 3a. Simultaneous growth of ZnO in all

directions (longitude branch elongation and radial shell formation) was also reported previously.[18] Finally, Zn_2GeO_4 nanowire heterostructures with ZnO shells and aligned branches were developed after growth of ~60 min (Figures 1 and 3).

Zn_2GeO_4 nanowires were selected as the substrates to demonstrate the crystallographic alignment, since they facilitate detail epitaxial characterizations and more importantly they are single-crystalline substrates. It is believed that aligned ZnO nanorod arrays could also be grown on Zn_2GeO_4 microcrystals or bulk crystals with uniform crystal structure. The rectangular $Zn_2GeO_4(1\bar{1}0)$ lattice is analogous to the $Al_2O_3(110)$ plane, which exhibits small lattice mismatches with the ZnO *c*-plane and promotes heteroepitaxial growth. However, the semiconducting nature of Zn_2GeO_4 crystals makes them more attractive substrates for potential device applications, such as light-emitting diodes and UV light sensors.

4. Conclusions

In conclusion, we have demonstrated the successful growth of aligned ZnO nanorod arrays on lattice-matched Zn_2GeO_4 nanocrystals. The single-crystalline Zn_2GeO_4 nanowires serve as ideal substrates to investigate the crystallographic relationship with ZnO nanorods. Detailed HRTEM analyses revealed that the perpendicular orientations of the ZnO branches were driven by heteroepitaxial growth between the ZnO *c*-plane and Zn_2GeO_4 side facets. Structure defects such as misfit dislocations were observed at some of the interfaces to release the strain. Due to the small lattice mismatch with ZnO at specific planes, the semiconducting Zn_2GeO_4 crystals would potentially serve as promising substrates for ZnO nanorod array growth, as well as device applications.

Acknowledgment. The authors thank X. W. Lu, P. Darmawan, M. Y. Chan, and N. Singh for their support and insightful discussions. We also thank S. C. Lim and J. Guo for their technical support.

Supporting Information Available: Schematic illustrations of the furnace setup and crystal lattice structures. This material is available free of charge via the Internet at http://pubs.acs.org.

References and Notes

(1) Li, Y.; Qian, F.; Xiang, J.; Lieber, C. M. *Mater. Today* **2006**, *9*, 18.
(2) Agarwal, R.; Lieber, C. M. *Appl. Phys. A: Mater. Sci. Process.* **2006**, *85*, 209.
(3) Huang, M. H.; Mao, S.; Feick, H.; Yan, H. Q.; Wu, Y. Y.; Kind, H.; Weber, E.; Russo, R.; Yang, P. D. *Science* **2001**, *292*, 1897.
(4) Fan, Z. Y.; Wang, D. W.; Chang, P. C.; Tseng, W. Y.; Lu, J. G. *Appl. Phys. Lett.* **2004**, *85*, 5923.
(5) Liu, C. H.; Zapien, J. A.; Yao, Y.; Meng, X. M.; Lee, C. S.; Fan, S. S.; Lifshitz, Y.; Lee, S. T. *Adv. Mater.* **2003**, *15*, 838.
(6) Law, M.; Greene, L. E.; Johnson, J. C.; Saykally, R.; Yang, P. D. *Nat. Mater.* **2005**, *4*, 455.
(7) Qin, Y.; Wang, X. D.; Wang, Z. L. *Nature* **2008**, *451*, 809.
(8) Greene, L. E.; Law, M.; Tan, D. H.; Montano, M.; Goldberger, J.; Somorjai, G.; Yang, P. D. *Nano Lett.* **2005**, *5*, 1231.
(9) Gu, Z. J.; Paranthaman, M. P.; Xu, J.; Pan, Z. W. *ACS Nano* **2009**, *3*, 273.
(10) Wang, X. D.; Song, J. H.; Li, P.; Ryou, J. H.; Dupuis, R. D.; Summers, C. J.; Wang, Z. L. *J. Am. Chem. Soc.* **2005**, *127*, 7920.
(11) Kuykendall, T.; Pauzauskie, P. J.; Zhang, Y. F.; Goldberger, J.; Sirbuly, D.; Denlinger, J.; Yang, P. D. *Nat. Mater.* **2004**, *3*, 524.
(12) Anoop, G.; Krishna, K. M.; Kumar, K. R.; Jayaraj, M. K. *J. Electrochem. Soc.* **2008**, *155*, J270.
(13) Lewis, J. S.; Holloway, P. H. *J. Electrochem. Soc.* **2000**, *147*, 3148.
(14) Yan, C. Y.; Lee, P. S. *J. Phys. Chem. C* **2009**, *113*, 14135.
(15) Zhang, X. M.; Lu, M. Y.; Zhang, Y.; Chen, L. J.; Wang, Z. L. *Adv. Mater.* **2009**, *21*, 2767.
(16) Chen, C. H.; Chang, S. J.; Chang, S. P.; Li, M. J.; Chen, I. C.; Hsueh, T. J.; Hsu, C. L. *Chem. Phys. Lett.* **2009**, *476*, 69.
(17) Wang, D.; Qian, F.; Yang, C.; Zhong, Z. H.; Lieber, C. M. *Nano Lett.* **2004**, *4*, 871–874.
(18) Mazeina, L.; Picard, Y. N.; Prokes, S. M. *Cryst. Growth Des.* **2009**, *9*, 1164.
(19) Bae, S. Y.; Seo, H. W.; Choi, H. C.; Park, J. *J. Phys. Chem. B* **2004**, *108*, 12318.
(20) Wang, X. D.; Song, J. H.; Wang, Z. L. *J. Mater. Chem.* **2007**, *17*, 711.
(21) Nikoobakht, B.; Eustis, S.; Herzing, A. *J. Phys. Chem. C* **2009**, *113*, 7031.
(22) Vandermerwe, J. H.; Bauer, E. *Phys. Rev. B* **1989**, *39*, 3632.

JP909068V